Journal of the Energy Institute 109 (2023) 101287

Contents lists available at ScienceDirect

Journal of the Energy Institute

journal homepage: www.elsevier.com/locate/joei

Pyrolytic-gasification of biomass and plastic accompanied with catalytic sequential tar reformation into hydrogen-rich gas

Babalola Aisosa Oni [a,*], Samuel Eshorame Sanni [b], Anayo Jerome Ibegbu [c], Olusegun Stanley Tomomewo [a], Humphrey Nwenenda Dike [d]

[a] Department of Energy Engineering, University of North Dakota, 58202, USA
[b] Chemical Engineering Department, Covenant University, Km 10 Idiroko Road, PMB 1023, Ota, Nigeria
[c] Department of Mechanical Engineering, Madonna University, Elele, Nigeria
[d] Department of Petroleum Engineering, Covenant University, Km 10 Idiroko Road, PMB 1023, Ota, Nigeria

ARTICLE INFO

Handling Editor: Dr. Paul Williams

Keywords:
Hydrogen-rich gas
Catalytic reforming
Polypropylene
Pyrolysis
Gasification

ABSTRACT

Synthetic Fe–CaO–Ni-mayenite-CeO_2 catalyst was adopted in the production of H_2-rich gas from formed tar obtained from biomass-plastic pyrolysis and gasification. The molar ratio of the individual components in the catalyst (Fe–CaO–Ni-mayenite-CeO_2) is 1:1:1: 1:2 as designed for the catalytic reforming of tar. The steam flow rate was fixed at 0.5 g/min. The role of mayenite-CeO_2 in the catalyst and the temperature at which the catalyst was calcined during the pyrolysis–gasification of the Hazelnut shell/polypropylene mixture was examined. The inclusion of Mayenite was to provide the desired support for the activity of Ni–Fe. In addition, sulfur poisoning influences the activity of the Fe–CaO–Ni-Mayenite catalyst. On the other hand, CaO can easily become deactivated by biomass-tar, hence the reason it was impregnated with Fe along with Mayenite which was present on the surface of the catalyst's support as evidenced by the result from characterization. As a promoter, CeO_2 improves nickel's resistance to carbon deposits while also boosting its sulfur tolerance. The activity of the catalyst was also monitored at varying space velocities, temperatures, steam to carbon ratios, residence times and particle sizes. The production of H_2-rich gas was achieved at 1000 °C using 30 wt% of the catalyst.

1. Introduction

Biomass has gained recognition as a sustainable source of energy that can be used to replace fossil fuels [1]. Biomass offers a number of advantages, owing to its being a carbon-neutral source of energy, its availability, and its variety of uses [2]. Steam biomass gasification has spurred a lot of interest among its competitive hydrogen sources, owing to it being a potential source of H_2-rich gas form producer gas, which is useful for a variety of applications, including power generation and combined heat applications [3], electricity generation, especially in fuel cells, etc. [2]. Therefore, removing the impurities obtained from pyrolysis-gasification is critical in order to make the resulting gas useful. To remove particles and tar, a gas conditioning and cleaning system is required. Tar is made up of a variety of chemical molecules, the majority of which are aromatic hydrocarbons. As a result, catalytic steam reforming is an efficient approach to reducing tar formation and increasing hydrogen production from biomass gasification.

H_2 has been produced from biomass and waste plastics via thermal processing. However, because the hydrogen yield from biomass is usually low, adding high-H_2-content polymers to the feed stock (biomass) increases the yield of H_2 in the output stream [6]. There have been reports of different biomass-plastic co-pyrolysis combinations that produce H2, such as pine cone-polystyrene, wood-polypropylene, and pine cone-polyethylene. These reactions took place in different reactors with different catalysts that helped increase the hydrogen yield [5]. Despite these processes, the hydrogen yield is still low, and not much significant hydrogen yield was seen due to the process of pyrolysis due to the reaction steps [4,7].

Catalysts such as Ni–CaO–C, Ni–Al_2O_3; Ni–Mg–Al–Ca have been investigated for plastic and biomass gasification [1,6,9]. Owing to their strong performance and low-cost implications during H_2 generation, Ni-based catalysts are an attractive choice among the list of apt catalysts for reforming processes at elevated temperatures [3,10]. Due to their high surface areas, commercial Ni catalysts are frequently used in tar steam reforming processes, although they are easily deactivated due to sulfur poisoning [11], carbon deposition [3], and sintering [1]. Carbon

* Corresponding author
E-mail address: oni.babalola@und.edu (B.A. Oni).

https://doi.org/10.1016/j.joei.2023.101287
Received 18 February 2023; Received in revised form 14 May 2023; Accepted 15 May 2023
Available online 16 May 2023

deposition is a significant source of Ni catalyst deterioration [1,4,7,11]. Deactivation difficulties can be addressed by altering specific aspects of the catalyst; for example, sintering can be reduced by the formation of solid bonds between the catalyst-support and active phases, which prevent nickel particles from migrating and agglomerating on the surface of the catalyst [8,11], but too strong interactions decrease the reducibility of NiO species, which results in a drop-in catalyst activity.

The deposition of carbon on nickel catalysts has been extensively researched [1,7,9,11], and some potential solutions include using catalyst supports/promoters that possess high oxidative characteristics, which help to gasify/oxidize the carbon deposits with the intent of abating catalyst deactivation [6].

Owing to its ability to accommodate free oxygen species, mayenite ($Ca_{12}Al_{14}O_{33}$) possesses a crystalline nanoporous structure with increased oxidative characteristics [13]. According to Hosono et al. [14], mayenite crystals have an inverse zeolitic nature with anion-accommodating properties. In the reformation of tars, Ni/Mayenite has demonstrated an impressive performance, where in a space of a few hours, the hybrid catalyst indicated a sloping decline in CH_4 conversion. Li et al. [15] used a Ni/$Ca_{12}Al_{14}O_{33}$ catalyst in a fixed-bed reactor to facilitate steam reforming of toluene (a reference tar chemical). They discovered its moderate resistance to the formation of coke and the poisoning of H_2S. As a result, mayenite has been shown to be efficient in preventing carbon deposition on the active surface of nickel without being able to prevent sulfur poisoning, although $Ca_{12}Al_{14}O_{33}$ has no CO_2 sorption properties, except with the addition of CaO.

Due to their advantageous thermodynamic and chemical features, CaO-based materials have been proclaimed as solid sorbents for CO_2 capture [5,12,16]. The main issue with CaO is that its sorption capacity drops dramatically after multiple carbonation-calcination cycles [17]. Hydration of the sorbent, optimization of calcination conditions [8], and deposition of CaO on an inert support [4] are some of the methods used to reduce sorbent efficiency loss due to sorption cycles and diffusion effects. $CaAl_2O_4$ [18], $Ca_2Fe_2O_5$ [19], and $Ca_{12}Al_{14}O_{33}$ (Mayenite) [4, 14] have all been investigated for carbon dioxide sorption in the presence of CaO. Mayenite has no CO_2 sorption properties, but it has a stable network and a large surface area that prevent CaO from being deactivated via sintering [20]. Mayenite appears to be a good choice for CaO support. Its synthetic route has a significant impact on the characteristics (pore volume, surface area) of its associates in the referred composite [21].

Moisés et al. [22] used the microwave-assisted self-combustion approach to create Ni–CaO–$Ca_{12}Al_{14}O_{33}$ for carbon dioxide sorption via an accelerated steam methane reforming reaction. The heat balance of the global reaction was favored by the sorption of CO_2 by CaO, which moved the Water Gas Shift reaction (WGS) and steam reforming towards hydrogen generation. Vanga et al. [23] observed the dry reforming of CH_4 over 15 wt% Ni/CaO-mayenite in a micro-reactor at 600–800 °C under atmospheric conditions for 12 h at a weight hourly space velocity of 120 Lg-$^1h^{-1}$. The incorporation of CaO prevents coke deposits from forming on the surface of the catalyst, thus enhancing productivity. $Ca_{12}Al_{14}O_{33}$ has also been utilized in conjunction with a Fe catalyst by Zamboni et al. [24]. They used Fe/CaO/Mayenite as a catalyst in toluene steam reforming for H_2-rich gas production. The Fe encouraged the H_2 generation. However, sulfur poisoning has remained an issue of concern. CeO_2 is widely known for enhancing the stability and activity of Ni-based catalysts in the reforming of heavy tar [25]. On the catalyst's surface, cerium oxide functions as an O_2 donor, which strengthens the interaction between C and CO_2, thus assisting in the reduction of carbon deposition via the reverse Boudouard reaction [26]. Additionally, as Cesário et al. [27] noted, cerium promotion may become more pronounced in the presence of hydrogen sulfide, thus lowering the harmful effects of H_2S on the nickel active sites. In lieu of the aforementioned, sulfur poisoning has a negative influence on the Ni/Mayenite catalyst. Hence, CeO_2 was found to be an effective promoter of the catalyst, which helped in improving the carbon deposit resistance, nickel-sulfur tolerance, and deactivation resistance of the catalyst.

To generate hydrogen-rich gas during the steam reforming process, it is necessary to preserve the catalyst to increase its potential for Ni deactivation resistance at higher temperatures, reduce the presence of sulfur compounds, and capture CO_2. Furthermore, the use of the pyrolysis process alone may not give a significant yield of hydrogen-rich gas [3,7], likewise the gasification process [9] with the use of hazelnut shell polypropylene, hence the combination of both processes.

Ni–Fe was used as a catalyst for the production of H_2-rich gas; the inclusion of mayenite was to provide the desired support for the activity of Ni–Fe. CaO is beneficial for promoting H_2 composition. On the other hand, CaO can easily become deactivated by biomass tar, hence the reason it was impregnated with Fe along with mayenite, which was present on the surface of the catalyst's support as evidenced by the result from characterization. As a promoter, CeO_2 improves nickel's resistance to carbon deposits while also boosting its sulfur tolerance. Mayenite can help increase the total gas yield. Nevertheless, these two supports still have limitations. CaO is ineffective for increasing hydrogen yield but adsorbed the composition of CO_2 which influences the water-gas-shift (WGS) reaction, thereby increasing the H_2 yield. Because increasing yields of other gases reduce hydrogen composition, the hydrogen composition of product gases is comparatively lower when Ni–Fe is used. As a result, a novel idea is proposed to mix these two supports (CaO and Mayenite) to maximize their advantages while minimizing their drawbacks in order to achieve high hydrogen yield and composition. The new Fe–CaO–Ni-mayenite-CeO_2 catalyst has mayenite and CaO as catalyst support and CeO_2 as a promoter to activate the core Ni–Fe. The results show that the synergistic effect of various constituents in the catalyst Fe–CaO–Ni-mayenite-CeO_2 can produce a high hydrogen yield and composition at the same time. However, polypropylene was admixed with biomass to evaluate the effectiveness of the new Fe–CaO–Ni-mayenite-CeO_2 catalyst. The use of Fe–CaO–Ni-mayenite-CeO_2 catalysts in tar reforming compounds under various operating conditions was investigated in this study. During the catalytic reforming process, the catalysts' resistance to sulfur poisoning was also assessed. The proposed catalyst was examined for its physico-chemical properties before being utilized for the reforming of tar from hazelnut shell-polypropylene. The catalyst was characterized by various techniques (XRD, XPS, SEM, BET, and TPD).

2. Materials and methods

2.1. Preparation of the catalyst

The Fe/CaO sorbents containing 10% Fe were produced by impregnation using an aqueous precursor. At 900 °C, the Ca precursor (CaO) was calcined. $Fe(NO_3)_3.9H_2O$) was employed as the Fe salt. The nitrate salt was dissolved in distilled water, and then the calcined calcium oxide was introduced and agitated until a suspension was formed. The mixtures were dried in an oven at 110 °C for 24 h and crushed to a fine powder after solvent evaporation at 70 °C. The material was further calcined for 3 h at 900 °C at a rate of 3 °C/min.

Also, the preparation of Mayenite began with the preparation of the precursor, $Ca(CH_3COO)_2$, and powdered aluminum oxide. Aluminum oxide was initially ground for 2 at 200 rpm in a ball mill (Pulverizete-8, Fritch). All the aforementioned chemicals were purchased from Sigma Aldrich. Under constant agitation at 80 °C, $CaCO_3$ (equivalent to a molar ratio of $CH_3COOH/CaCO_3 = 9$) was added to a mixture containing acetic acid and water (1:0.5); CO_2 was emitted during the $Ca(CH_3COO)_2$ synthesis as indicated in (1)

$$CaCO_3 + 2CH_3COOH \rightarrow Ca(CH_3COO)_2 + H_2O + CO_2 \quad (1)$$

There was no carbon dioxide released after the reaction was completed. Crushed Aluminum oxide was introduced in a stoichiometric ratio during the synthesis of $Ca(CH_3COO)_2$. The resulting slurry was

then oven dried at 105 °C for 24 h. The resulting $Al(OH)_3$ and Ca $(CH_3COO)_2$ mixture was crushed in a mortar and further calcined at 700 °C for 4 h to decompose it to pure CaO; the resulting reaction are as depicted in (2) and (3).

$$Ca(CH_3COO)_2 \rightarrow CaCO_3 + CH_3COCH_3 \quad (2)$$

$$CaCO_3 \rightarrow CaO + CO_2 \quad (3)$$

$Ca_{12}Al_{14}O_{33}$ was obtained by calcining the resulting components for 4 h at 1000 °C

The previously obtained $Ca_{12}Al_{14}O_{33}$ powder was ground in a mortar for the synthesis of Ni/$Ca_{12}Al_{14}O_{33}$ and sieved between 20 and 40 mm. Ni catalyst was then added to make the Ni/$Ca_{12}Al_{14}O_{33}$ powder by the method of impregnation with $(Ni(NO_3)_2.6H_2O)$ diluted in water while stirring the mixture vigorously at 55 °C. The amount of nickel(II) nitrate hexa-hydrate salt used to make the desired catalyst with 5% Ni was determined. The resultant slurry was oven-dried for 12 h at 105 °C and calcined for 2 h at 900 °C. The catalyst was then crushed and sieved between 15 and 40 mm.

To deposit 20 wt % of CeO_2 on the catalyst, a portion of the Ni/$Ca_{12}Al_{14}O_{33}$ was also impregnated with an aqueous solution of $(Ce(NO_3)_3.6H_2O)$. Wet impregnation with CeO_2 was performed in a similar way as Nickel impregnation, and the compound was then calcined at 800 °C for 4 h [6]. Having produced the Ni/$Ca_{12}Al_{14}O_{33}$/CeO_2 by the aforementioned technique, the Ni/$Ca_{12}Al_{14}O_{33}$/CeO_2 powder was sieved using a 15–40 mm mechanical sieve.

Finally, the already prepared Fe/CaO was admixed with Ni/$Ca_{12}Al_{14}O_{33}$/CeO_2 to obtain the required catalyst for the tar reforming process. The mixed ratio of the components that make up the Fe–CaO–Ni-mayenite-CeO_2 = 1:1:1: 1:2 respectively, which makes up the best ratio for high yield of gaseous components. This was achieved after several trial mixed ratios/proportions of the components (i.e., 1:1:1:1:1:1; 1:2:1:1:1; 1:1:2:1:1:1 etc.) were tested in the tar reforming process to achieve high hydrogen yield.

2.2. Biomass material and composition

The typical biomass material that was employed in this study is hazelnut shell. The aim of choosing the hazelnut shell is due to its carbon content and volatile matter; it also contains an appreciable amount of H_2 as presented in Tables 1 and 2. A Carlo Erba Flash EA 1112 elemental analyzer was used to evaluate the S, C, N, H, and O content (Table 1) of the biomass. The proximate analysis of the hazelnut shell was performed using a Shimadzu TGA-50H instrument. Weight loss was correlated with volatile and moisture content at 105 °C and between 105 and 900 °C, respectively. Air was introduced into the sample for the purpose of determining the fixed carbon content, which combusts and leaves an ash residue. The polypropylene (Table 2) was supplied by BP Chemicals, UK, in the form of 1.0 mm virgin polymer pellets.

Table 1
Ultimate/proximate analysis of Hazelnut shell.

Ultimate analysis/wt.%			
Carbon[b]	Oxygen[b]	Nitrogen[b]	Hydrogen[b]
49.70	45.20	0.09	4.00

Proximate analysis/wt.%[a]			
Ash[c]	Volatile[c]	Moisture[a]	Fixed carbon[c]
0.9	75.1	5.4	19.5

[a] On wet basis.
[b] Dry-ash-free basis.
[c] Dry basis.

Table 2
Properties of polypropylene.

	Polypropylene (PP)
Ultimate analysis	
O_2 (%)	0
C (%)	86.1
N (%)	0
S (%)	0.01
H (%)	12.7
Moisture (%)	1.1
Ashes (%)	0.1
Devolatilization temperature (°C)	410
Particle density (kg/m^3)	938
Low heating value (kJ/kg)	45,000
Bulk density (kg/m^3)	565
Initial devolatilization temperature (°C)	240
Diameter and thickness of fuel pellets (mm)	5.0

2.3. Pyrolysis–gasification experiments

Pyrolysis-gasification tests on a mixture of hazelnut shell and polypropylene were conducted in two individually heated electric furnaces using a two-stage stainless tube reactor setup (Fig. 1). At the first stage, the pyrolysis was conducted, and the generated volatile compounds were sent straight into the second stage reactor, where the pyrogas were steam gasified alongside the catalysts. In the pyrolyzer, a sample holder consisting of 3 g of sample (2 g of hazelnut shell and 1 g of polypropylene) was introduced at the first stage. The reactor where the pyrolysis process took place was kept at 700 °C with a constant nitrogen supply. The pyrolysis reactor was heated at 40 °C/min with a temperature of 600 °C in the catalyst gasification stage (1st stage) with steam fed into the reactor from a steam generator at a feed rate of 0.5 g/min. The pyrolysis gases were brought into the gasification reactor using N_2 as a carrier gas, where they were reacted with steam and the catalyst. Unreacted water and oil were collected using a condenser. Gas chromatography (GC) was used to evaluate the non-condensed gases contained in the gas sample bag. Establishing the weights of the condenser, sample holder, and syringe before and after the experiments helped in the determination of the amounts of char, injected water, and condensed liquids. The investigations were carried out in triplicate to guarantee that the results were repeatable. A GC (Agilent 8860GC) analyzer with a flame ionization detector (GC-FID) and a thermal conductivity detector (GC-TCD) was used to evaluate the product gases collected in the gas sample-bag. The GC-TCD indicated the amount of H_2, CO_2, CH_4 and CO released from the gasified/pyrolyzed raw material. After each test, the amount of tar formed was quantified using an Agilent GC-MS. The catalyst's performance was tested at 700, 800, 900, and 1000 °C.

2.4. Characterization of catalyst

2.4.1. X-ray diffraction (XRD)

XRD analysis was carried out on the samples (XRD 600, Shimadzu-X-ray-diffractometer, Japan) with CuK radiation (20 mA, 50 kV) in the 2 range of 10–80°, with 0.05° resolution within 2 s. The phase of the catalyst was determined from the Crystallography Open Database.

2.4.2. N_2 adsorption isotherms and scanning electron microscopy (SEM)

In a Surface Area and Pore Size Analyzer, N_2 adsorption at 77 K was used to determine the pore diameter, surface area, and pore volume (Quanthrome Industries, Novak, US) of the catalyst. Prior to testing, the samples were outgassed for 20 h under vacuum conditions at 350 °C. The BET method was used to calculate the surface area, while density functional theory (DFT) was used to calculate the pore size distribution. The SEM model Prisma E SEM, Thermo Fisher Scientific, USA, was used to analyze the morphology of the catalyst at different elevated temperatures.

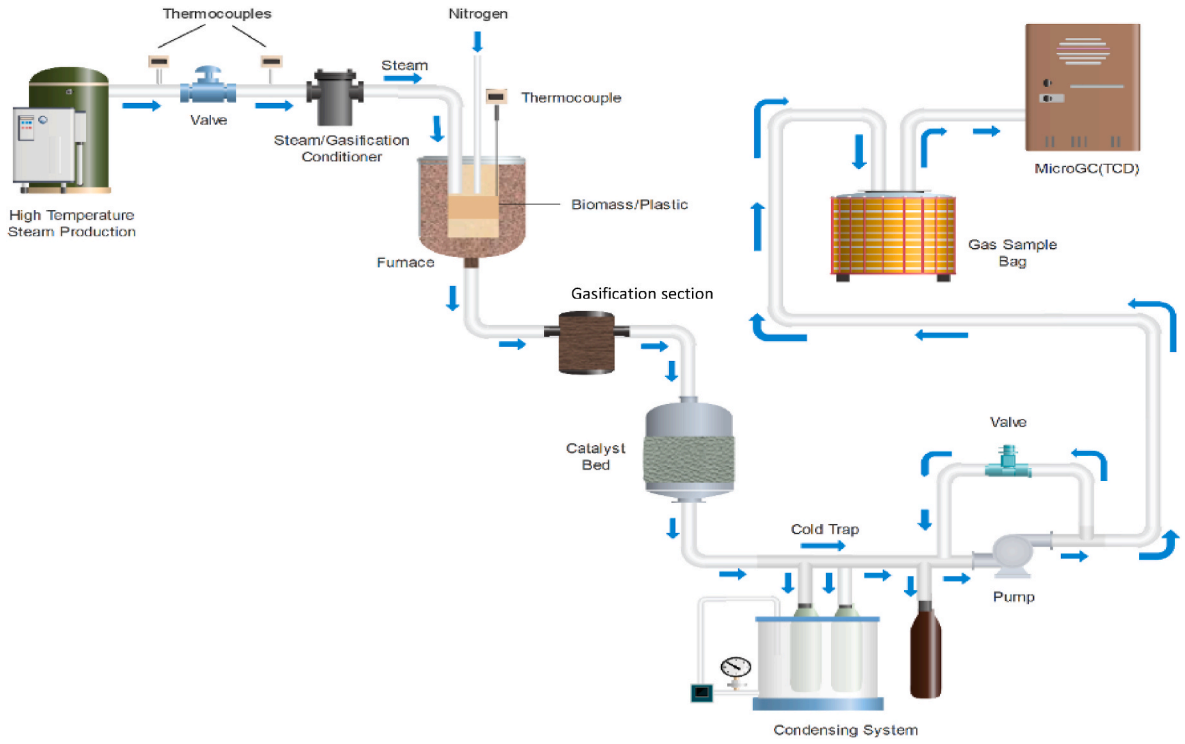

Fig. 1. Schematic set up of Pyrolysis–gasification using Fe–CaO–Ni-mayenite-CeO_2 catalyst.

2.4.3. XPS, FTIR, TEM, H_2-TPR and TPD- NH_3/CO_2 analysis

Images of the TEM were captured using a Philips CM-2000 microscope operating at 200.0 kV. An Automatic Chem II 2900 computer with a TCD conductor was used to perform the H_2-TPR (TCD). 50 mg of the catalyst was heated to 150 °C (at an interval of 10 °C/min) under Ar (Core-gas Ar, >99.9%) for 30 min before being cooled to 40 °C (at a temperature reduction rate of 5 °C/min). The samples were heated to temperatures between 50 and 850 °C at a rate of 10 °C/min while being infused with 5 vol % H_2 in Ar at a 50 mL/min. TPD- NH_3/CO_2, was used to study the basicity and acidity of the catalyst. 50 mg of the material was analyzed using the Automatic Chem II 2900 machine. The catalysts were pre-treated for 30 min at 200 °C (5 °C/min) under Helium (Core-gas, >99.9%), and then cooled to 40 °C (at 5 °C/min). The samples were further saturated for an hour at 20 mL/min with Core-gas, 5.1% ammonia, ammonia-helium or Core-gas carbon dioxide, 1% carbon dioxide nitrogen. By flushing the catalyst with helium for 1 h and then heating it from 40 to 800 °C at 10 °C/min, physisorbed molecules were eliminated. VG Scientifics ESCALAB250 type X-ray photoelectron spectroscopy was used to investigate the elemental composition and valence states of the ions that were located on the surface of the catalyst. A Bruker Vectors 20 (Ettligen, Germany) was used to conduct the FTIR spectra at 28 °C with a wavenumber resolution of 1/cm at a frequency range of 4000–400/cm. 32 scans were run and averaged in order to obtain a good signal-to-noise ratio.

3. Results and discussion

3.1. Evaluation of Fe–CaO–Ni-mayenite-CeO_2 performance

3.1.1. Effect of temperature

The presence of mayenite and other components of the catalyst was detected using XRD analysis of the reduced catalyst. In Fig. 2, a small quantity of Fe–CaO–Ni-mayenite-CeO_2 phase was detected at a low temperature (600 °C). The peak of the Fe–Ni phase dropped when the temperature increased to 700 °C, and the signal of Fe–CaO–Ni-mayenite-CeO_2 began to develop; this process persisted until it reached 900 °C.

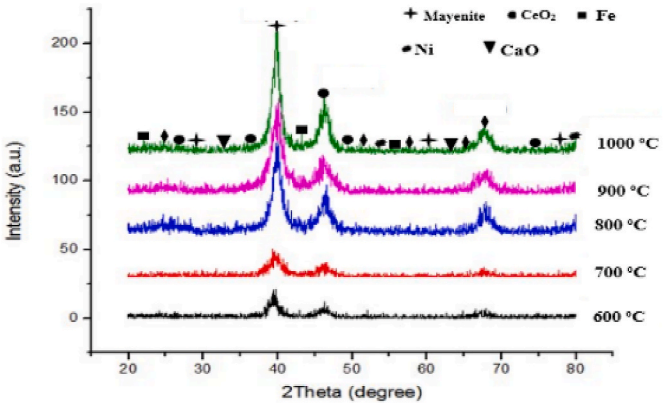

Fig. 2. XRD patterns of Fe–CaO–Ni-mayenite-CeO_2 at different temperatures.

The XRD pattern displays the peaks of pure Fe–CaO–Ni-mayenite-CeO_2 when the temperature increases up to 1000 °C, thus indicating that the Fe–CaO–Ni-mayenite-CeO_2 was successfully synthesized. All of these findings show that, under the conditions used in this study, the temperature at which the Fe–CaO–Ni-mayenite-CeO_2 was fully formed was 1000 °C. According to Kumagai et al. [7], the utilization of biomass/plastic as a carbon source has the potential to promote water gas formation; thus, the use of biomass/polypropylene materials promotes water gas formation. This is attributed to the reducing gases (CO and H_2) generated during biomass/plastic pyrolysis. At 53.5° and 79.7°, the calcined catalysts also displayed typical reflections of crystalline Ni. After CeO_2 impregnation and calcination, the sample Fe–CaO–Ni-mayenite-CeO_2 gave reflections that correspond to the crystalline CeO_2 at 27.3°, 36.4°, 46.1°, 48.7°, and 74.4°. Mayenite gave the maximum peak in the pattern, thus indicating good stability and high dispersion on the catalyst-support, and excellent Mayenite synthesis, which is consistent with the results from previous research [62, 63]. Also, despite some reflection of crystalline CaO (32.7°, 63.6°) in the

diffractograms, calcium segregation occurred throughout the catalyst's preparation-phase. The crystalline reflection of Fe displayed by the calcined catalyst are at 22.3°, 43.7°, and 55.5°.

3.1.2. Effect of Fe–CaO–Ni-mayenite-CeO_2 loading

To ascertain the effect of Fe–CaO–Ni-mayenite-CeO_2 loading on the biomass/plastic, 10–30 wt% of Fe–CaO–Ni-mayenite-CeO_2 was considered. The samples were calcined at 1000 °C for 3 h and characterized by XRD. The XRD patterns of the calcined products prepared using 10–30 wt % load of Fe–CaO–Ni-mayenite-CeO_2 are illustrated in Fig. 3. It was discovered that the highest catalytic activity of CaO-Mayenite was attained at an initial loading of 10 wt%, and the indicators of the Fe–CaO–Ni-Mayenite-CeO_2 phase increased as the CaO-Mayenite amount increased as a result of the improved crystallinity of the Fe–CaO–Ni-Mayenite-CeO_2 particles. Further increase in the loading of CaO-mayenite amount to 30 wt%, displayed the Fe–CaO–Ni-mayenite-CeO_2 crystalline phases. This may have occurred as a result of excess loading of CaO-mayenite. Navarro et al. [28] reported similar results, where they studied the effect of the CaO-mayenite loading on the crystalline CaO-mayenite-phases during calcination at 1000 °C, the results showed that at high CaO-mayenite loading, higher quantities of CaO-mayenite were required to form the Fe–CaO–Ni-mayenite-CeO_2 catalyst. Thus, according to the results obtained from the XRD patterns, the catalyst is most active at 1000 °C, with 30 wt% load for the reforming of tar, to achieve H_2-rich gas.

3.2. BET surface area and pore volume of Fe–CaO–Ni-mayenite-CeO_2 catalyst

The BET surface area and pore volume of the Fe–CaO–Ni-mayenite-CeO_2 catalyst with various wt.% loading onto the biomass-polypropylene reactor are described in Table 3. The pore volumes and surface areas of the samples first increase and then decrease with variation in the catalyst/biomass-plastic loading ratio. All samples showed large surface areas, which are advantageous to the catalyst; however, the 30 wt% catalyst loaded onto the desired biomass-polypropylene ratio displayed the highest surface area, which corroborates with the works of [6], indicating that higher loading of catalyst/biomass ratio between 10 and 30 wt% catalyst results in a high surface area. The porosity of the catalyst can be described by adsorption isotherms with N_2. The size distribution of the catalyst is important to ensure that both reactants and products are transported efficiently to and from the active sites of the catalyst. Smaller sizes are also used in some catalyst systems to control adverse reactions. By comparing used and fresh catalysts, size

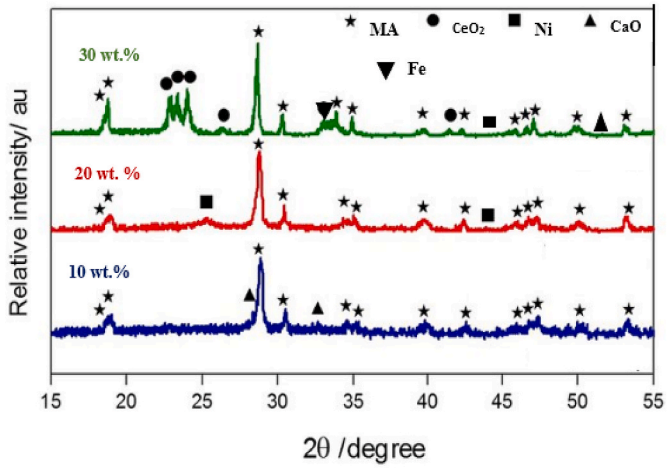

Fig. 3. XRD patterns at different % wt. Loading (Reaction temperature 1000 °C).
MA* (Mayenite).

Table 3
Surface area and pore volume of different catalyst load (wt.%) at 1000 °C.

Loading amount (wt.%)	Pore volume (cm^3/g)	Surface area (m^2/g)
10	0.195	89.4
20	0.202	93.7
30	0.233	109.1
35	0.209	88.3

Table 4
Textural properties of the novel (Fe–CaO–Ni-mayenite-CeO_2) catalyst used at different temperatures.

Parameter	600 °C	700 °C	800 °C	900 °C	1000 °C	1100 °C
Pore volume (cm^3/g)	0.21	0.29	0.36	0.44	0.58	0.48
BET Surface area (cm^2/g)	80.8	87.2	91.3	96.8	105.7	129.9
Pore size (nm)	1.40	1.03	1.33	1.35	1.42	1.41
Micropore surface area (m^2/g)	11.8	12.5	14.1	14.9	16.4	15.3

distribution and pore volume can be used to identify such processes (see Table 4).

The SEM images of the catalyzed biomass-propylene reaction at various tar reforming temperatures are as given in Fig. 4. The SEM images of the catalyst at 600 °C, displayed less pores, however, as the temperatures increases, the pores of the catalyst begin to open between 800 and 900 °C, due to the elemental distribution of the catalyst as confirmed by the XRD pattern distribution. Higher pore opening was noticed at 1000 °C, where most of the biomass/plastic on the catalytic bed are converted to gaseous product which are highly enriched in hydrogen. It was noticed that further increase in the temperature did not produce higher hydrogen-rich gas, instead it was reduced, due to pore closure of the catalyst. Thus, high hydrogen-rich gas was attained at 1000 °C (Figs. 5 and 6), based on the catalyst/feedstock mixture which justifies the works of refs [4,8].

3.3. Characterization of the catalyst using FT-IR (Fe–CaO–Ni–$Ca_{12}Al_{14}O_{33}$ –CeO_2)

An investigation of an oxide catalyst's surface hydroxyl structure can thus give vital information on the oxide surface and its interaction with surface metal atoms, which frequently involves surface OH groups. The surface hydroxyl structure was studied at various catalyst loadings (10, 20, and 30% wt.%). The catalyst OH stretching region displays a series of bands dominated at 2921 cm^{-1} and a weak shoulder at 2987 cm^{-1}, both of which are defining features of OH groups on the surface of the catalyst as described by Refs. [13,19]. When mayenite is added to Fe–CaO–Ni–CeO_2, the intensity of these OH stretching bands, particularly those of the shoulder bands, is seen to decrease; this is in line with refs [6,27]. The sharp OH stretching band was supplemented by a broader band at 1635 to 1695 cm^{-1} when the loading of the catalyst was raised from 10% to 30%, suggesting that the OH groups on the 30% Fe–CaO–Ni-mayenite-CeO_2 are now bonded to more electronegative surface metal atoms than others. Mayenite-OH is responsible for these OH groups. As a result of these findings, mayenite-CeO_2 is widely dispersed on the Fe–CaO–Ni surface. It also implies that mayenite-CeO_2 primarily interacts with the Fe–CaO–Ni surface via bonding, which is consistent with the XRD patterns. The C–H stretching vibration is assigned to those at 1450 cm^{-1}. The stretching vibration of the C═O bond is responsible for the 929 cm^{-1} band. The band at 477 cm^{-1} corresponds to the phenyl ring's C–H bond stretching vibration. Other absorption peak transitions are caused by methyl groups reacting with mayenite hydroxyl groups.

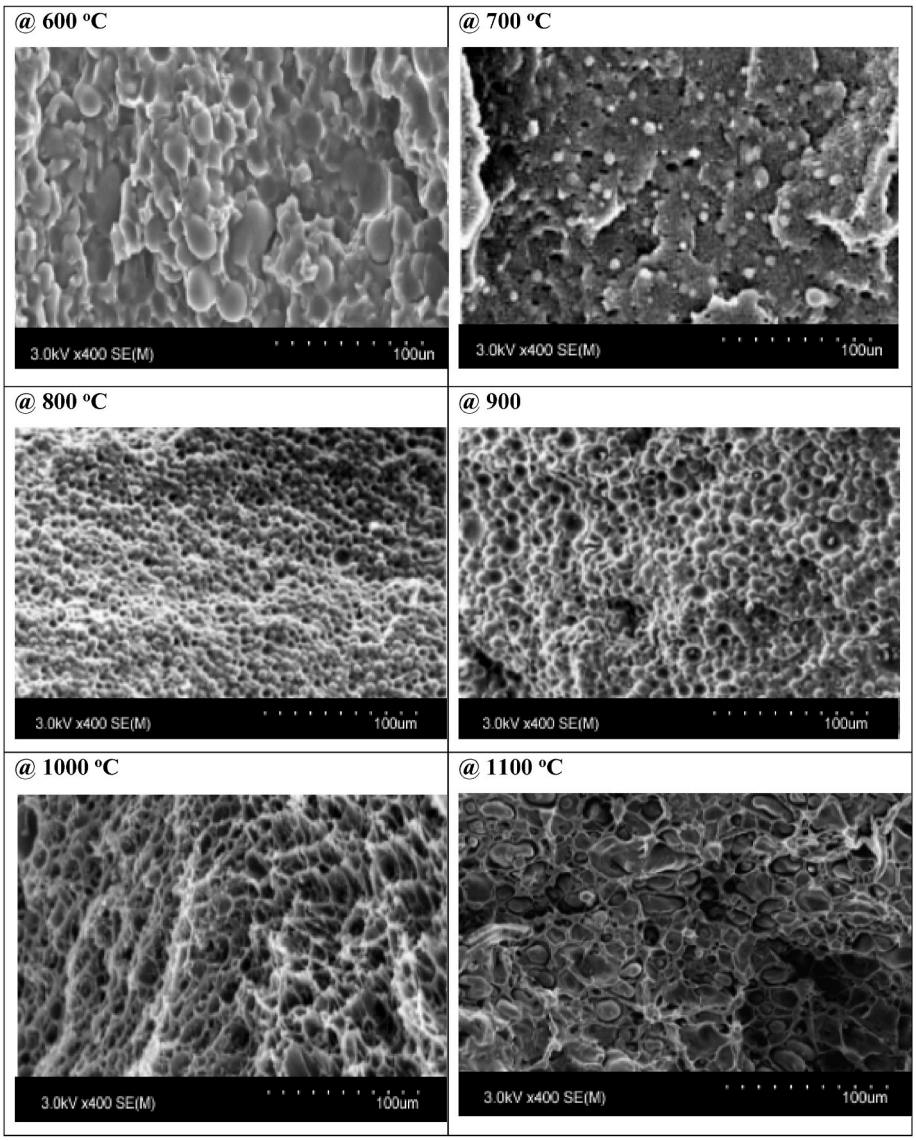

Fig. 4. SEM images of catalyst to biomass-propylene at different temperature.

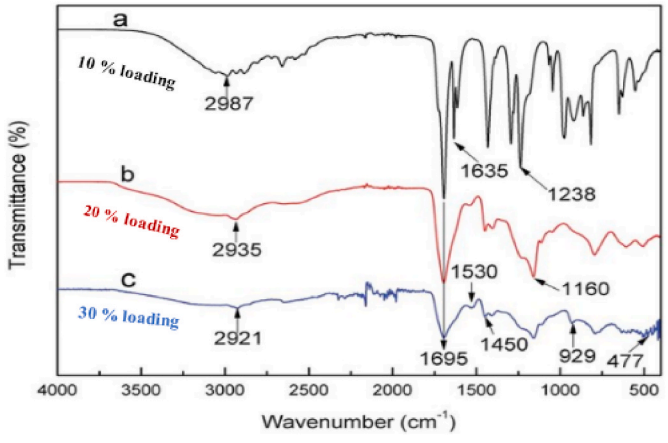

Fig. 5. FT-IR of spent catalyst for sequential tar reformation into hydrogen-rich gas at different loading conditions.

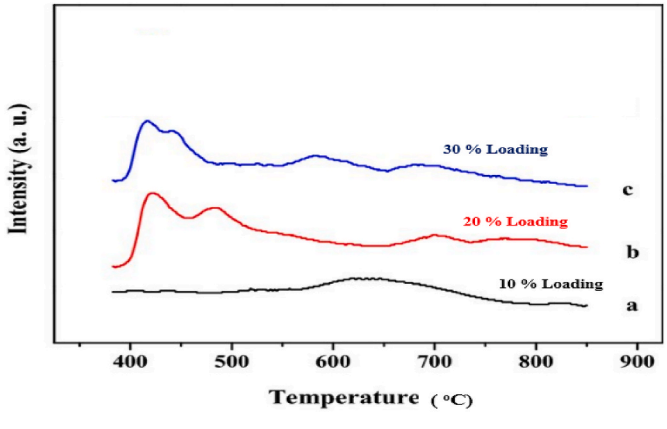

Fig. 6. NH_3 TPD of the catalyst.

3.4. *NH_3 TDP of the catalyst*

An excellent NH_3-catalyst should have sufficient acid sites to boost ammonia adsorption and activation at active sites during the reaction

[16]. As a result, the NH_3-TPD was carried out to study the acid properties of Fe–CaO–Ni-mayenite-CeO_2. TPD peaks were noticed at around 410 and 415 °C in Fe–CaO–Ni-mayenite-CeO_2, which may be attributed to ammonia desorbed from the catalysts' weak, medium, and strong acid sites as described by Moisés et al., [22]. The higher temperature peak is caused by ammonia desorption from catalytic active acid sites. It is thought that there is interaction between the mayenite and the acid sites of the catalyst, weakening their acid strength. Higher loading of the catalyst resulted in a lower peak at about 700 °C, however, there was no further increase in peak as the catalyst loading increased. Since large peak was noticed at 30% loading of the catalyst, it can be attributed to ammonia adsorbed on the surface of the catalyst, as earlier reported by Xu et al., [20]. The differences in acid densities of Fe–CaO–Ni-mayenite-CeO_2 can be primarily attributed to the differences in their percentage loadings. An increase in the loading percentage to a higher percentage had no effect on the peaks.

3.5. The H_2-TPD of the catalyst

The numbers of active sites of reduced Fe–CaO–Ni-mayenite-CeO_2 were determined by H_2-chemisorption and H_2- TPD. The peaks can be seen in the patterns, as shown in Fig. 7. Between 92 and 110 °C, the first peaks occurred and were assigned to the weak active site, and a broad peak around 510 °C could be found over the catalysts, which corresponds to the strong active site having strong H_2 adsorption, this result justifies the work of ref. [13]. With variations in percentage loading, the temperature of three hydrogen desorption peaks varied. The maximum temperature of hydrogen desorption peaks on the Fe–CaO–Ni-mayenite-CeO_2 catalyst, with 110 and 516 °C, indicated strong hydrogen adsorption to the active sites, which may be attributed to the increase in the number of active sites and the high distributions of nickel as demonstrated by Ref. [27]. Given the possibility of TPD spill-overs onto the surface of the catalysts, pulse chemisorption of hydrogen was also performed. At 30% Fe–CaO–Ni-mayenite-CeO_2 catalyst, the highest nickel dispersion was noticed, which was higher compared to 20% Fe–CaO–Ni-mayenite-CeO_2 catalyst. The amount of hydrogen adsorbed on 10% Fe–CaO–Ni-mayenite-CeO_2 catalysts decreased significantly, implying that the amounts of Ni decreased, resulting in their lower catalytic activity.

3.6. The CO_2-TPD of the catalyst

TPD of CO_2 was performed to determine the basic site strength and distribution, and the resulting CO_2 desorption profiles of 10, 20, and 30% wt.% catalysts are shown in Fig. 8. The basicity of Fe–CaO–Ni-mayenite-CeO_2 has an influence on the performance of the catalytic reaction due to CO_2 acidic nature. According to Vanga et al. [23], a strong basic site improves the catalytic activity and increases the reaction of reacting gases and chemisorption. When the basic sites are

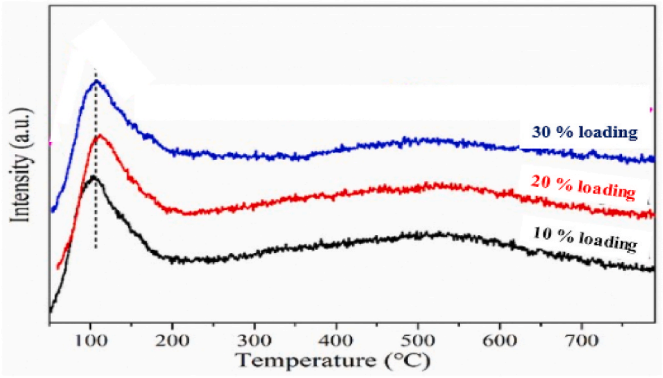

Fig. 7. H_2-TPD of Fe–CaO–Ni-mayenite-CeO_2 loading catalyst.

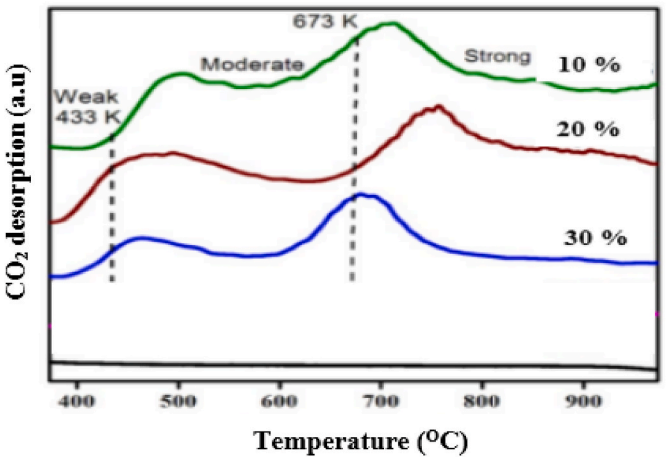

Fig. 8. CO_2-TPD profile of Fe–CaO–Ni-mayenite-CeO_2 catalyst.

distributed on the catalyst, they correspond to the various desorption peaks in the CO_2-TPD profile at temperatures of 400–450, 500–600, 600–700, and >800C for weak, intermediate, strong, and very strong [24]. Since the carbon dioxide desorption peaks appeared at nearly the same temperature range, all the test catalysts displayed the same classification of the basic active site. At 600 °C, all catalysts showed an elbow peak. The peak intensities increased and then decreased as the adsorption temperatures increased (Fig. 8), achieving the highest values at around 700 °C. The laboratory results revealed that the CO_2 adsorption capacities of mayenite-based catalysts' CO_2 improved in the following order: 10 wt%, 20 wt%, and 30 wt%, in accordance with the XRD patterns. The CO_2 TPD profiles of Fe–CaO–Ni-mayenite-CeO_2 catalysts show that basic sites occurred. The strong basic sites at temperatures between 600 and 700 °C of the catalysts were a result of CaO occurrence in the catalyst at 30% loading, and the variation in milder basic sites was prompted by CeO_2, which justifies the works of Huang et al. [11]. It was noted that the alkalinity of 10% Fe–CaO–Ni-mayenite-CeO_2 is weaker than others due to the lower peaking temperature (640–670 °C). Even though a portion of $Ca(OH)_2$ was converted to mayenite along with CeO_2 during the catalytic preparation method, the catalyst's alkalinity was weakened. Cesário et al. [27] revealed that a stronger CO_2 desorption peak around 500 °C indicated a strong CO_2 adsorption ability, which improved catalytic activity and performance. Furthermore, the CO_2 adsorption peak of strong basic sites shifted a bit higher with increased mayenite concentration, implying that mayenite promoted CO_2 adsorption. The increased surface basicity of the catalysts may promote CO_2 adsorption, resulting in a hydrogen-rich gas.

3.7. The TEM characterization of Fe–CaO–Ni-mayenite-CeO_2 catalyst

TEM images of the Fe–CaO–Ni-mayenite-CeO_2 catalyst are presented in Fig. 8. All of the catalysts had a particle size distribution ranging from 3 to 4.8 nm. Nickel was more evenly distributed on the catalyst surface, with particle sizes of 3.0 nm for the 30% wt. Nevertheless, the particle size distribution of nickel was uneven on the 20% catalyst, whereas there were large nickel particles visible on the 10% catalyst. Oni et al. [8] demonstrated that the particle size distribution of nickel affects the surface area of a heterogeneous catalyst. The nickel distributions supported by the CaO-mayenite-CeO_2 catalyst were revealed by TEM analysis. Substantial volumes of nickel particles aggregated in the 10% Fe–CaO–Ni-mayenite-CeO_2 sample due to the lower surface area, as shown in Fig. 9. Nickel particles are evenly distributed in the Fe–CaO–Ni-mayenite-CeO_2 sample (30 wt%) as a result of their surface area. A histogram of the nickel particle size distribution is also shown. The catalyst particle size follows the trend: 10 wt%

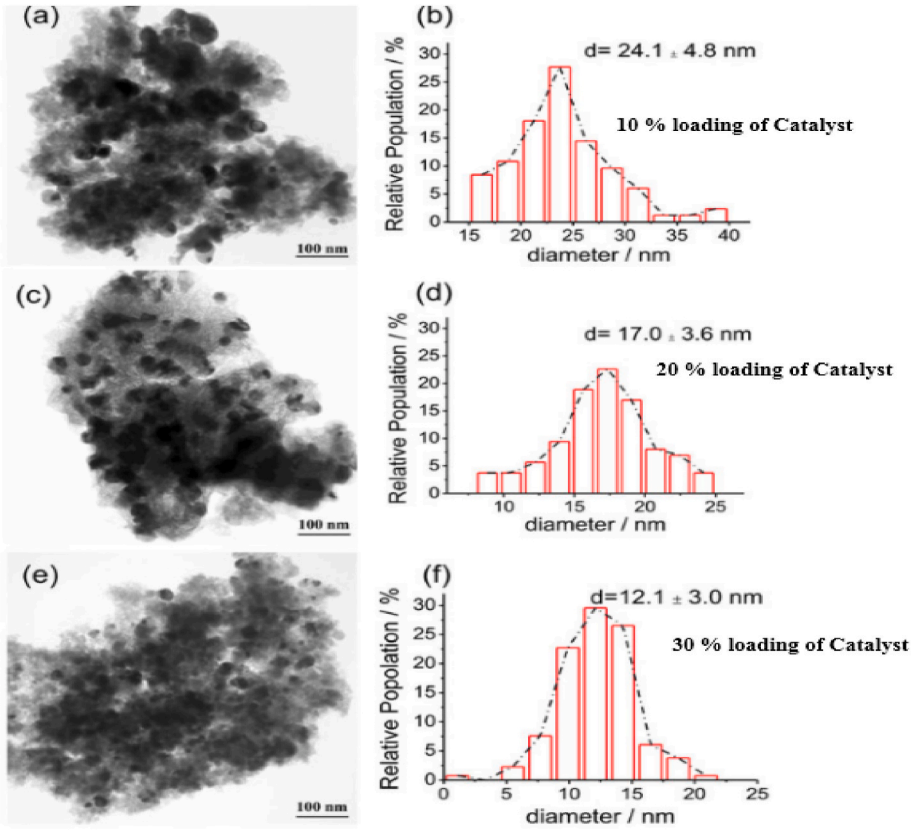

Fig. 9. TEM characterization of Fe–CaO–Ni-mayenite-CeO_2 catalyst.

Fe–CaO–Ni-mayenite-CeO_2 > 20 wt% Fe–CaO–Ni-mayenite-CeO_2 > 30 wt% Fe–CaO–Ni-mayenite-CeO_2.

3.8. The X-ray photoelectron spectroscopy (XPS) characterization of Fe–CaO–Ni-mayenite-CeO_2 catalyst

XPS analysis of Fe–CaO–Ni-mayenite-CeO_2 showed Ni, Fe, Ce, Ca, M, and O species, with M representing mayenite. Fig. 10a shows Ce^{3+} and Ce^{4+} signals in the Ce 3d spectrum. The Ce $3d_{5/2}$ and Ce $3d_{3/2}$ peaks at

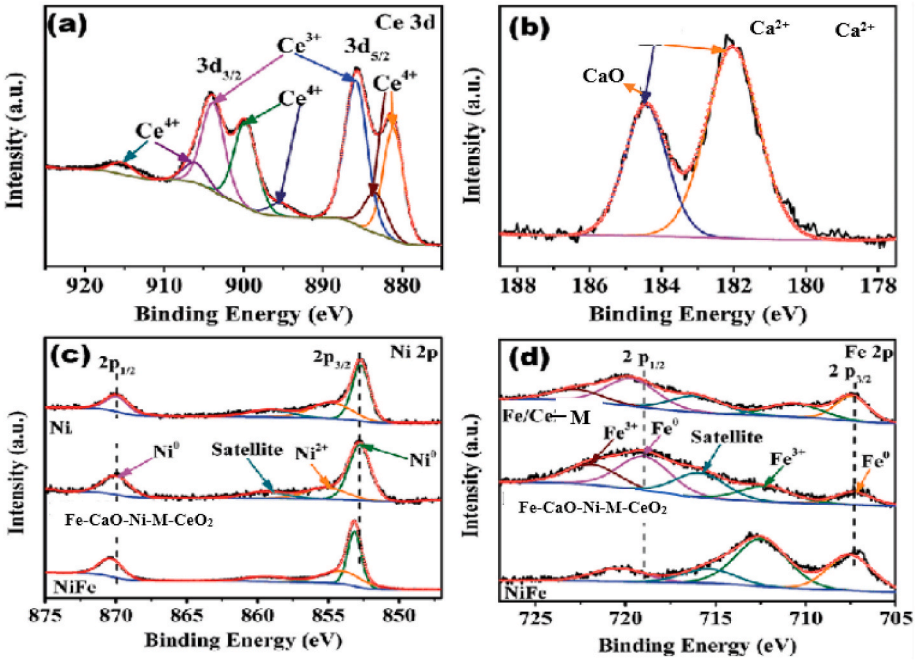

Fig. 10. XPS characterization of Fe–CaO–Ni-mayenite-CeO_2 catalyst.

898.9, 907.2, and 916.1 eV are assignable to Ce^{4+}, while the peaks at 886.4 and 902.7 eV are Ce^{3+}. CaO causes Ca^{2+} peaks at 181.9 and 185.0 eV in the Fe–CaO–Ni-mayenite-CeO_2 catalyst (Fig. 10b). The Fe–CaO–Ni-mayenite-CeO_2 catalysts higher CaO binding energy suggests that Ca^{2+} donates electrons. Fig. 10c and d shows Ni $2p_{3/2}$ and Ni $2p_{1/2}$ peaks at 853.1 and 869.8 eV for Fe–CaO–Ni-mayenite-CeO_2. Fe^0 assigns Fe $2p_{3/2}$ and Fe $2p_{1/2}$ signals at 708.2 and 719.9 eV. The Ni $2p_{3/2}$ peaks at 856.1 eV and Fe 2p peaks at 711.9 and 723.2 eV are assigned to Ni^{2+} and Fe^{3+}, which may be due to air oxidation of surface Ni–Fe NPs during sample processing. The satellite peaks are also the Ni $2p_{3/2}$ peaks at 858.7 eV and Fe at 716.5 eV. Due to increased electron density in metal centers, the binding energies for Fe 2p and Ni 2p and in Fe–CaO–Ni-mayenite-CeO_2 were negatively shifted compared to pure Ni–Fe NPs. The Ni 2p peaks of Fe–CaO–Ni-mayenite-CeO_2 also shift to a higher binding energy, while the Fe 2p levels shift negatively, confirming the construction of a Ni–Fe alloy. Electronic transport between CaO, Ni, Fe, and mayenite-CeO_2 solid solutions in the Fe–CaO–Ni-mayenite-CeO_2 catalyst boosts catalytic activity and tar reformation into hydrogen-rich gas. Thus, the bimetallic catalyst exhibits higher selectivity and activity for hydrogen gas due to the synergistic effect on electron interaction between the nickel and iron as shown by the XPS.

3.9. Effect of steam to biomass/plastic ratio on the yields of the product gas @ 1000 °C

Steam reforming of tar with Fe–CaO–Ni-mayenite-CeO_2 at an average biomass/polypropylene particle size of 0.045 mm was tested at 1000 °C with steam to biomass/plastic ratios of 0, 0.5, 1, 1.5, and 2, as illustrated in Fig. 11, in order to determine the effect of steam reforming of tar on the yields of product gas. The hydrogen content of the product gas improved to 81.1% vol% as the amount of steam injected increased, whereas the CO content (11.53 vol%) increased while the amount of CO_2 remained basically unchanged at a low level. In general, the amount of tar converted with steam injection is determined by the catalysts' properties. These findings, corroborate those of previous reports [Li et al., [16]; Sun et al., [17]; Xu et al. [21]], which suggest that increasing the steam to biomass/plastic ratio, results in an increase in the biomass/plastic conversion rates. This implies that as the amount of injected steam increased, the Fe–CaO–Ni-mayenite-CeO_2 became more active, thus activating the water gas shift reaction, which subsequently resulted in an increase in H_2 production.

The effect of the catalyst weight ratio (30 wt%) to biomass-polypropylene on the product gas yields from the catalytic pyrogasification of biomass-polypropylene is shown in Fig. 12. The experiments were carried out at 1000 °C. The findings demonstrated that the catalyst-to-biomass-polypropylene ratio had a significant impact on the product gas yields, particularly for hydrogen. Increasing the catalyst to biomass weight ratio will result in an increase in the yield of hydrogen

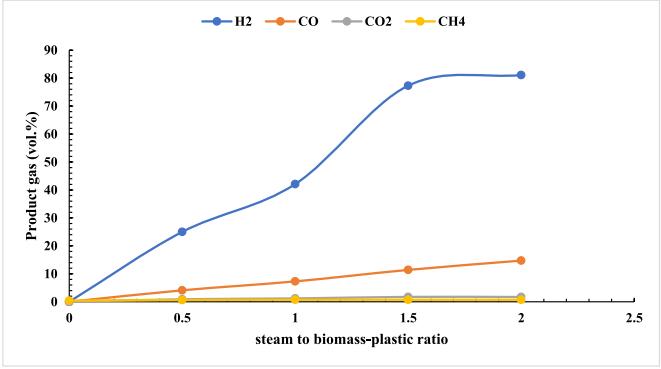

Fig. 11. Effect of steam to biomass/polypropylene ratio on product gas yield for the Fe–CaO–Ni-mayenite-CeO_2 @ 1000 °C.

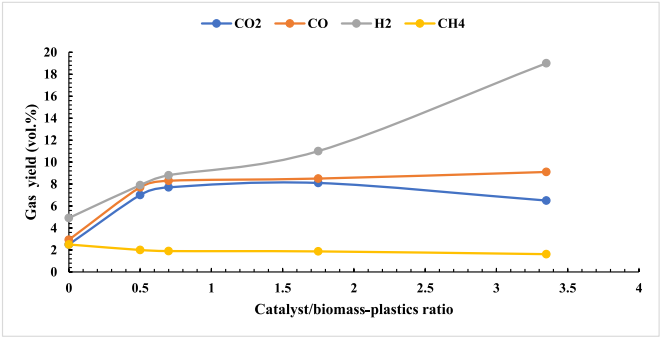

Fig. 12. Effect of catalyst to biomass-plastic ratio on the gas production yields at 1000 °C.

compared to that of CO, CO_2 and CH_4 respectively. According to Kumagai et al. [7], the addition of catalyst to biomass-based plastics can result in a high hydrogen yield. Furthermore, when the catalyst-to-biomass weight ratio is 2, the CO yield increases. This could be a result of the water-gas shift reaction's considerable influence. Hence, it can be inferred that the Fe–CaO–Ni-mayenite-CeO_2 catalyst is very active for this reaction. Furthermore, high hydrogen-rich gas can be obtained at a weight ratio of biomass-polypropylene to catalyst above 3.35 (Fig. 12); this result corroborates the findings of refs [14,25].

3.10. Effect of particle size on H_2 yield

The yield of H_2 produced by steam tar reforming was compared in Fig. 13 based on the size of biomass-plastic feed. At varying temperatures, three different size categories (i.e., 0.0450 mm, 0.0450–0.50 mm, and 0.50–1.0 mm) of biomass-plastic were tested. Due to the higher surface area to volume ratio provided by lower particle sizes, lower particle sizes of the biomass-polypropylene feed resulted in an increase in H_2 yield. Oni et al. [8], demonstrated that smaller particle size of biomass with catalyst addition increases the hydrogen yield. The lowest size of catalyst (0.045 mm) demonstrated almost two times higher H_2 yield than the largest biomass/plastic size of 0.5–1 mm at 1000 °C; these results are justified by those of refs [29].

3.11. Catalytic effect of Fe–CaO–Ni-mayenite-CeO_2

In this section, the pyrolysis bed was heated up to 1000 °C, and Fe–CaO–Ni-mayenite-CeO_2 was fed as catalyst onto the bed. The bed temperature was between 600 and 1000 °C under a weighted hourly space velocity of 0.3 h^{-1} so as to understand the catalytic effect of Fe–CaO–Ni-mayenite-CeO_2 on the product stream.

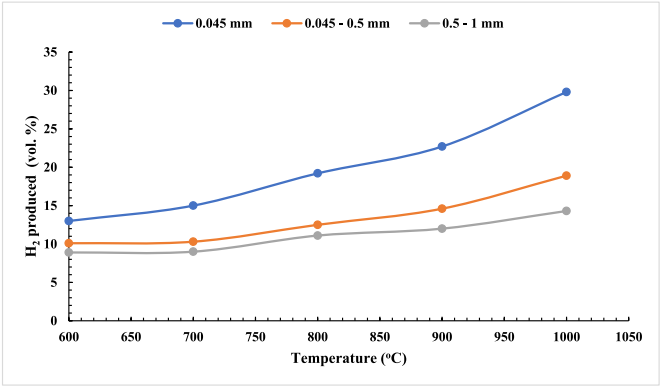

Fig. 13. Effect of biomass-plastic sizes on hydrogen yield with 30 wt % catalyst @ 1000 °C.

3.11.1. The influence of the catalyst on the yield of pyrolysis products

Fig. 14 shows the temperature effects on the pyrolysis products' distribution of hazelnut shell/polypropylene when the Fe–CaO–Ni-mayenite-CeO2 catalyst was used as a catalyst. At 600 °C, the gas yield increased significantly by an average of 32.3 vol% compared to the case of no catalyst. When the reactor increased from 600 °C to 1000 °C, the gas yield increased as well, from 77.1 to 87.8 vol%, with a decrease in the tar yield as the temperature increased. At 1000 °C, the tar yield decreased to 0.3 vol%, reaching approximately zero. The amount of char also decreased by an average of about 9 vol%, regardless of the influence of the temperature and catalyst. This is because the char yield was affected by the operating conditions and inherent activities within the pyrolysis-gasification bed. According to Palma et al. [26], most catalytic beds affect only the gas and tar yield by thermally decomposing volatile organic gases and catalytically reforming gaseous products. The analysis indicated that Fe–CaO–Ni-mayenite-CeO_2 seemed to have a superior catalytic influence on the removal of tar, with a tar removal rate of about 100% at 1000 °C. The tar generated was converted into gaseous products by the catalytic effect of Fe–CaO–Ni-mayenite-CeO_2, which corroborates the work of refs. [17,25]. The temperature in blank condition was maintained at 600 °C.

3.11.2. Catalyst effect on gas composition

The effect of catalyst-temperature on gas composition is illustrated in Fig. 15. The gaseous products generated include CO_2, CO, H_2, and CH_4. With the inclusion of the Fe–CaO–Ni-mayenite-CeO_2 catalyst, the amounts of H_2 and CO produced increased, while those of CH_4 and CO_2 decreased. With the temperature of the reactor increasing, there was a constant increase in the amount of H_2 and CO, while the amount of CH_4 and CO_2 decreased at 600–1000 °C. At 600 °C, the amounts of H_2 and CO reached their maximum values of 30.1% and 25.3%. The values nearly doubled the results obtained for the case involving no catalyst. It is quite interesting to find that hydrogen generation is favored by increased temperatures. Researchers [3,5,11,19,24] have shown that an increase in temperature during the gasification reaction favors a high amount of hydrogen yield. Yet higher catalytic temperatures will be prone to lead to sintering and aggregation of metallic active sites, especially the Ni site, which often result in dehydrogenation. By contrast, the value of CO_2 decreased from 20.1% (no catalyst) to 11.4% (at 600 °C) and further decreased to 7.1% (at 1000 °C). The amount of CH_4 showed a similar trend decrease with the inclusion of catalyst at elevated temperatures. The increase in CO and H_2 can be attributed to the boosting of the decomposition of tar under the rising reactor-temperature. Interestingly, the H_2 composition kept increasing but remained almost stable at 1000 °C, after which there was no further increase even at 1100 °C. The results show that H_2 was consumed at a higher temperature, which could be due to pyrolysis-gasification reactions like hydrogasification and the reverse of dry methane reforming. The decrease in the amount of CH_4 and CO_2 confirmed that secondary gas-phase reactions became more intense with the continuous increase in the reactor-temperature

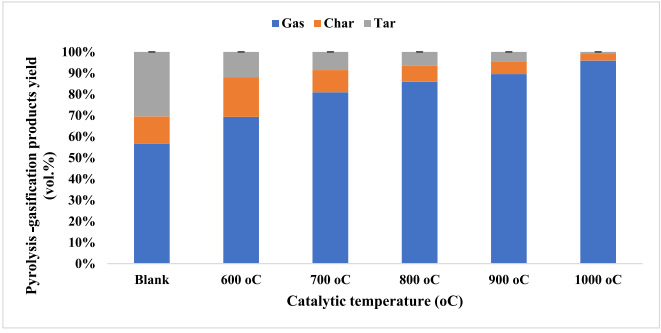

Fig. 14. Effect of temperature on the distribution of pyrolysis-gasification products of Hazelnut shell/polypropylene.

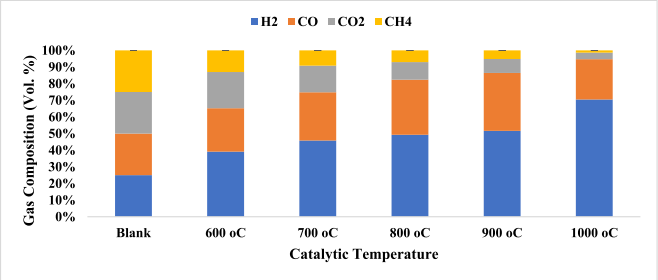

Fig. 15. Effect of temperature of catalyst on gas composition of Hazelnut shell/polypropylene.

[12]. The results revealed that a rise in temperature influenced the catalyst's (Fe–CaO–Ni-mayenite-CeO_2) activity, which then improved the secondary gas reactions and increased the quantity of H_2 and CO in gas streams. Table 5 presents the quantitative value of gas composition obtained at optimum temperature conditions compared with the literature data.

3.12. Reaction mechanism of Fe–CaO–Ni-mayenite-CeO_2 during tar reforming reaction

Because benzene and other aromatic compounds are not produced during the Fe–CaO–Ni-mayenite-CeO_2 catalytic reforming reaction of tar, the tar is totally transformed into gaseous products after adsorption onto the active sites of the catalyst. It then permeates the pores of the catalyst after tar adsorption. In addition, the reaction occurs at the pores' interior to produce the gaseous products, thus resulting in internal diffusion of the gases through the pores of the catalyst, which is preceded by outer diffusion of gases to the surface of the catalyst, and finally desorption of product gases from the catalyst's pore mouth, thus releasing H_2, CO, CO_2, and CH_4 [22,28]. Analyzing the reaction mechanism and catalyst in the catalyst removal stage is challenging due to the obvious complexity of tar -composition. Tar molecules are adsorbed onto the surface of the catalyst and thus generate radicals or intermediates. Gasifying agents, such as steam, can be adsorbed on the catalyst's surface, which may then dissociate into free radicals that are then desorbed along with the formation of the product gases [12,24]. The catalyst's pore structure and content of mayenite and CeO_2 improve the reforming process' efficiency. Mayenite provides a high specific surface area, strong thermal and chemical stability, and improved catalyst performance throughout the reforming process; CeO_2 also provides mechanical stability to the Fe–CaO–Ni-mayenite system. Tar molecules initially diffuse into the internal pores of the catalyst through the catalyst's mesopores/micropores. Using mayenite and CeO_2 as promoters and supports, the tar molecules are adsorbed on the catalyst's surface and thus disintegrate into radicals. The generation of radicals is the first phase and the rate-determining step of the reaction. The catalyst's inclusion of CaO, mayenite, and CeO_2 weakens tar molecules, thus making it easy for them to be broken down into radicals. Aromatic

Table 5
The quantitative value of gas composition obtained at optimum temperature conditions compare with the literature data.

Feedstock/ Optimum temperature (°C)	Catalyst	CO (%)	CO_2 (%)	CH_4 (%)	H_2 (%)	Refs.
Sunflower/1000	$Ni/Ca_{12}Al_{14}O_{33}$	29	12	8	61	[15]
Plastics/900	Fe–Ni–MCM-41	25	11	7	57	[21]
Sawdust/1000	Fe/Ca/Ni	22	11	4	63	[29]
Wood sawdust/ 1100	Fe(III)/CaO	25	5	3	67	[30]
Wheat straw/ 1000	Fe–CaO–Ni-mayenite-CeO_2	24	4	2	70	**This study**

compounds with fused rings are easily broken down since they are relatively active (Fig. 16). Tar dissociated radicals can react with steam active radicals to generate microscopic tar molecules, including H_2, CO, and C_xH_y which cause tar compounds to reform [27]. The catalyst support and promoter mechanism become degraded as the reforming reaction continues to advance at higher temperatures (Fig. 15) above 1000 °C. Due to a lack of active sites at the last phase of tar reforming, the rate of radical production is significantly reduced at this state due to a drop in the performance of the catalyst [22]. According to Carlo et al. [5] and Sisinni et al. [1], high-temperature Ni–Fe sintering causes catalyst degradation, the loss of the active surface of the catalyst, and pore contraction due to the synergistic effect of encapsulation of Ni–Fe as a result of rapid agglomeration and the collapse of the support structure in the Ni crystal. Because Ni sintering occurs at elevated temperatures, it is necessary to include another catalyst support that prevents Ni sintering at high temperatures [25]. The permeability, porosity, and average pore size of Ni were maintained at 700–1000 °C in the presence of mayenite and CeO_2, which in turn served to stabilize the catalyst and prevent the degradation of the catalyst during the reforming process of tar.

3.13. Regeneration of Fe–CaO–Ni-mayenite-CeO_2 catalyst

Fig. 15 illustrates the product gas yields when the 30 wt% catalyst was used for steam reforming of biomass-polypropylene tar with and without catalyst-regeneration. Due to the reforming process, the produced gas yields were reduced marginally in the absence of catalyst-regeneration. As a result, the used catalyst needs to be regenerated before reuse so as to maintain its activity. Several experiments were carried out in an argon atmosphere at different temperatures (600, 700, 800, 900, and 1000 °C) in order to regenerate the deactivated Fe–CaO–Ni-mayenite-CeO_2 catalyst that was used in this study, which occurs as a result of sintering and carbon deposits. As a result, the spent catalyst was regenerated in an argon environment for 3 h at a temperature above 900 °C, and the catalyst's activity is as depicted in Fig. 17. The produced gas yield was found to be slightly lower than the original value, thus demonstrating that the used catalyst's catalytic activity was restored after use. Furthermore, residual tar may transport a portion of the alkaline earth metals and alkali species from the biomass-polypropylene and thus deposit them on the catalyst's surface, which in turn may result in increased catalyst-activity [23]. Based on the results, the Fe–CaO–Ni-mayenite-CeO_2 catalyst demonstrated good catalyst-activity and reusability after 5 cycles.

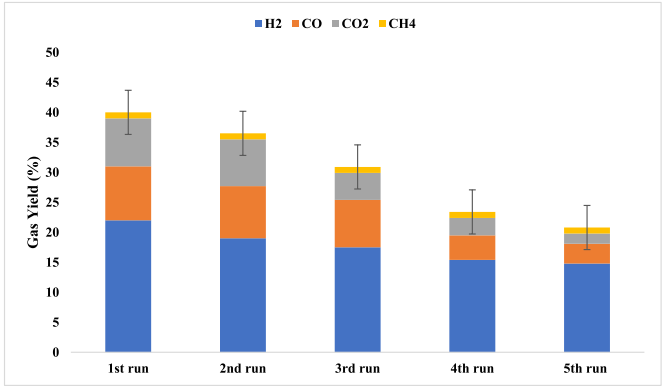

Fig. 17. Regeneration of 30 wt% Fe–CaO–Ni-mayenite-CeO_2 catalysts in steam reforming of tar from biomass-plastic at 1000 °C.

4. Conclusion

The effectiveness of the Fe–CaO–Ni-mayenite-CeO_2 catalyst in tar reforming at varying temperatures has been investigated in order to increase H_2 production from the pyrolysis-gasification of a hazelnut shell and polypropylene mixture. The Mayenite synthesis and the impregnation of Ce, Ni, Fe, and CaO were achieved, as evidenced by the catalysts' characterization patterns. After the pyrolysis–gasification trials, the metals were well disseminated in the catalyst, according to the XRD and other characterization results. The Fe–CaO–Ni-mayenite-CeO_2 showed increased pore volume, porosity, and surface area. The Fe–CaO–Ni-mayenite-CeO_2 catalyst was evaluated in a reactor under various operating conditions. At 1000 °C, the catalyst performed excellently in the reforming of tar. With the addition of a 30 wt% catalyst, the hydrogen yield was increased. The yield of hydrogen-rich gas increased for the smallest particle size (0.045 mm) of biomass-plastic compared to the cases involving larger particle sizes, thus implying that the presence of CaO in the catalyst reduces Ni particle agglomeration during the catalytic gasification process. In terms of steam to carbon ratio, a high H_2 yield was attained compared to other product gases. The gas and hydrogen yields were higher at shorter residence times of 0–10 s. The catalyst also showed improved tar reforming activity and reduced carbon deposition. The yield of gas produced was significantly influenced by the reaction temperature. Furthermore, the reaction mechanism, stability, and reusability of the catalyst (Fe–CaO–Ni-mayenite-CeO_2 catalytic) were also established. The catalyst was found to be efficient without a trace of residual/

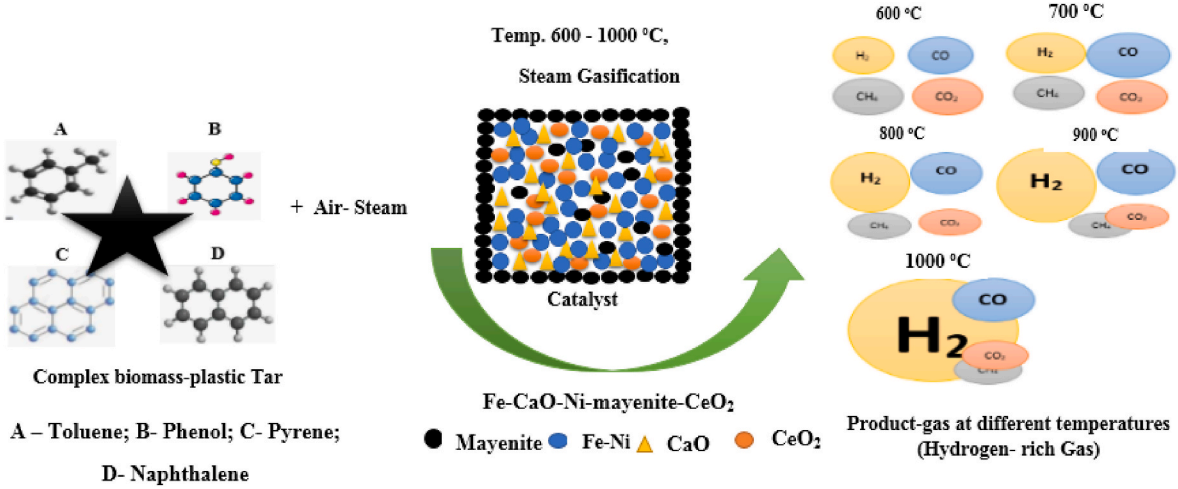

Fig. 16. Mechanism of reaction of tar reforming using **Fe–CaO–Ni-mayenite-CeO_2** for hydrogen-rich gas production.

unconverted tar, as observed under gas chromatography. After use, the Fe–CaO–Ni-mayenite-CeO_2 did not deactivate completely; however, it was active for a while after final regeneration.

Declaration of competing interest

The authors declare that they have no known competing financial interests or personal relationships that could have appeared to influence the work reported in this paper.

References

[1] M. Sisinni, A. Di Carlo, E. Bocci, A. Micangeli, V. Naso, Hydrogen-rich gas production by sorption enhanced steam reforming of wood gas containing TAR over a commercial Ni catalyst and calcined dolomite as CO_2, Sorbent (2013) 1–15, https://doi.org/10.3390/en60x000x.

[2] V. Pallozzi, A. Di Carlo, E. Bocci, M. Villarini, P.U. Foscolo, M. Carlini, Performance evaluation at different process parameters of an innovative prototype of biomass gasification amide to hydrogen production, Energy Convers. Manag. 130 (2016) 34–43, https://doi.org/10.1016/j.enconman.2016.10.039.

[3] B.A. Oni, S.E. Sanni, P.M. Ikhazuangbe, A.J. O Ibegu, Experimental investigation of steam-air gasification of Cymbopogon citratus using Ni/dolomite/CeO_2/K_2CO_3 as catalyst in a dual stage reactor for syngas and hydrogen production, Energy 237 (2021), 121542.

[4] C. Li, D. Hirabayashi, K. Suzuki, Development of new nickel-based catalyst for biomass tar steam reforming producing H2-rich syngas, Fuel Process. Technol. 90 (2009) 790–796.

[5] A.D. Carlo, D. Borello, M. Sisinni, E. Elisa Savuto, P. Venturini, E. Enrico Bocci, K. Kuramoto, Reforming of tar contained in a raw fuel gas from biomass gasification using nickel-mayenite-catalyst, Int. J. Hydr. energy. 40 (2015) 9088–9095.

[6] A. Di Giuliano, K. Gallucci, P.U. Foscolo, C. Courson, Effect of Ni precursor salts on Ni-mayenite catalysts for steam methane reforming and on Ni-CaO-mayenite materials for sorption enhanced steam methane reforming, Int. J. Hydrogen Energy 44 (2019) 6461–6480.

[7] S. Kumagai, J. Alvarez, P.H. Blanco, C. Wu, T. Yoshioka, M. Olazarc, P.T. Williams, Novel Ni–Mg–Al–Ca catalyst for enhanced hydrogen production for the pyrolysis–gasification of a biomass/plastic mixture, J. Anal. Appl. Pyrol. 113 (2015) 15–21.

[8] B.A. Oni, S.E. Sanni, S.O. Oyedepo, A.J. Ibegbu, Catalytic reforming of tar and volatiles from walnut shell pyrolysis over a novel Ni/olivine/La_2O_3 supported on ZrO_2, J. Energy Inst. 103 (2022) 33–46.

[9] E. Savuto, E. Navarro, R.M. Mota, N.A. Di Carloc, E. Boccid, M. Carlinia, J.L. G. Fierrob, Steam reforming of tar model compounds over Ni/Mayenite catalysts: effect of Ce addition, Fuel 224 (2018) 676–686.

[10] B.A. Oni, S.E. Sanni, O.A. Olabode, Production of fuel-blends from waste tyre and plastic by catalytic and integrated pyrolysis for use in compression ignition (CI) engines, Fuel 297 (2021), 120801.

[11] B. Huang, H. Chen, K. Chuang, R. Yang, M. Wey, Hydrogen production by biomass gasification in a fluidized bed reactor promoted by an Fe/CaO catalyst, Int. J. hydr. Energy. (2012) 6511–6518.

[12] Y. Liu, T. Chen, B. Gao, R. Meng, P. Zhou, G. Chen, Y. Zhan, W. Lu, H. Wang, Comparison between hydrogen-rich biogas production from conventional pyrolysis and microwave pyrolysis of sewage sludge: is microwave pyrolysis always better in the whole temperature range? Int. J. hydr. Energy. 46 (2021) 23322–23333.

[13] K. Shi, J. Yan, X. Luo, E. Lester, T. Wu, Microwave-assisted pyrolysis of bamboo coupled with reforming by activated carbon for the production of hydrogen-rich syngas, Energy Proc. 142 (2017) 1640e6, https://doi.org/10.1016/j.egypro.2017.12.543.

[14] H. Hosono, K. Hayashi, K. Kajihara, P.V. Sushko, A.L. Shluger, Oxygen ion conduction in 12CaO.7Al_2O_3. O^{2-} conduction mechanism and possibility of O^- fast conduction, Solid state Ionic 180 (55) (2009) 1–5.

[15] C. Li, D. Hirabayashi, K. Suzuki, Development of new nickel-based catalyst for biomass tar steam reforming producing H2-rich syngas, Fuel Process. Technol. 90 (2009) 790–796.

[16] M. Kaewpanha, G. Guan, Y. Ma, X. Hao, Z. Zhang, P. Reubroychareon, K. Kusakabe, A. Abudula, Hydrogen production by steam reforming of biomass tar over biomass char supported molybdenum carbide catalyst, Int. J. Hydrogen Energy 40 (2015) 7974–7982.

[17] Y. Sun, J. He, G. Yang, G. Sun, V. Sage, A review of the enhancement of bio-hydrogen generation by chemicals addition, Catalysts 9 (2019) 353.

[18] T. Xu, S. Bhattacharya, Direct and two-step gasification behaviour of Victorian brown coals in an entrained flow reactor, Energy Convers. Manag. 195 (2019) 1044–1055.

[19] K.-B. Park, Y.-S. Jeong, B. Guzelciftci, J.-S. Kim, Two-stage pyrolysis of polystyrene: pyrolysis oil as a source of fuels or benzene, toluene, ethylbenzene, and xylenes, Appl. Energy 259 (2020), 114240.

[20] T. Xu, J. Xu, Y. Wu, Hydrogen-rich gas production from two-stage catalytic pyrolysis of pine sawdust with calcined dolomite, Catalysts 12 (2022) 131.

[21] T. Xu, X. Zheng, J. Xu, Y. Wu, Hydrogen-rich gas production from two-stage catalytic pyrolysis of pine sawdust with nano-NiO/Al2O3 catalyst, Catalysts 12 (2022) 256, https://doi.org/10.3390/catal12030256.

[22] R.C. Moisés, S.B. Braúlio, C. Claire, M.A.M. Dulce, K. Alain, Catalytic performances of Ni–CaO–mayenite in CO2 sorption enhanced steam methane reforming, Fuel Process. Technol. 131 (2015) 247–253.

[23] G. Vanga, D.M. Gattia, S. Stendardo, S. Scaccia, Novel synthesis of combined CaO-Ca12Al14O33-Ni sorbent-catalyst material for sorption enhanced steam reforming processes, Ceram. Int. 45 (2019) 7594–7605.

[24] I. Zamboni, C. Courson, A. Kiennemann, Fe-Ca interactions, in: Fe-based/CaO Catalyst/sorbent for CO2 Sorption and Hydrogen Production from Toluene Steam Reforming, App. Cat. B: Environmental, 2017, pp. 154–165.

[25] B. Guzelciftci, K.-B. Park, J.-S. Kim, Production of phenol-rich bio-oil via a two-stage pyrolysis of wood, Energy 200 (2020), 117536.

[26] V. Palma, C. Ruocco, M. Cortese, M. Martino, Bioalcohol reforming: an overview of the recent advances for the enhancement of catalyst stability, Catalysts 10 (2020) 665.

[27] M.R. Cesário, B.S. Barros, Y. Zimmermann, C. Courson, D.M.A. Melo, A. Kiennemann, CO_2 sorption enhanced steam reforming of methane using Ni/CaO · Ca12Al14O33 catalysts, Adv. Chem. Lett. 1 (2013) 292–299, https://doi.org/10.1166/acl.2013.1037.

[28] B.A. Oni, S.E. Sanni, A.J. Ibegu, Production of light olefins by catalytic hydrogenation of CO2 over Y2O3/Fe-Co modified with SAPO-34, Applied Catalysis A, General 643 (2022), 118784.

[29] L. Qiuxian, L. Wei, Z. Xu, L. Ziliang, C. Qiue, X. Xiaoguang, Y. Shenfu, Experimental study on catalytic pyrolysis of biomass over a Ni/Ca-promoted Fe catalyst, Fuel (2019), 116690, https://doi.org/10.1016/j.fuel.2019.116690.

[30] C. Xu, S. Chen, A. Soomro, Z. Sun, W. Xiang, Hydrogen rich syngas production from biomass gasification using synthesized Fe/CaO active catalysts, J. Energy Inst. 91 (6) (2018) 805–816, https://doi.org/10.1016/j.joei.2017.10.014.